Standard Model Effective Field Theory: Applications in LHC Top Quark Physics

BSc dissertation

Xi Luo
The University of Manchester
10820021
xi.luo-5@student.manchester.ac.uk

Abstract

The Standard Model works as the 'best' model of matters we have based on the current experimental and theoretical knowledge. However, the SM still cannot explain everything. The Effective Field Theory (EFT) now serves as a tool to connect new physics ideas and experimental observations. This article introduces the Standard Model (SM) and Standard Model Effective Field Theory (SMEFT). It delves into the top sector application in SMEFT, highlighting its significance in probing potential new physics. Two specific top quark experimental analyses conducted in 2022 and 2023 using ATLAS data are presented, investigating the single quark generation and the $t\bar{t}Z$ process, respectively, which reveal detailed insights into the deviations from the SM predictions. Although they both improved the results and refined our understanding, neither analysis yields result consistent with the SM, showing no significant deviations.

1 Introduction

The Standard Model (SM) of particle physics is the dominant theoretical framework that describes the fundamental building blocks of the universe (quarks and leptons) and how they interact via electromagnetic, weak, and strong forces at the microscopic level [1]. This remarkable theory originated in the mid-20th century and has become a central pillar of modern physics. The Standard Model is an achievement that combines elegance and complexity and represents the culmination of decades of experimental and theoretical work.

In the mid-20th century, physicists explored the complex subatomic world and discovered countless particles. Due to the vast number of discoveries, Scientist faces challenges in explaining particle behaviour and fundamental forces, a unified theory began to take shape. In 1983, W and Z bosons existing in this theory were found experimentally, and the masses were consistent with those predicted in the Standard Model [2][3]. In the 1980s, the foundational elements of the Standard Model were laid out and validated. The latest achievement came in 2012 with the discovery of the Higgs boson [4], further cementing the Standard Model as a comprehensive description of the particle world.

While undeniably, the standard model is a very successful theory in the history of physics, it is still incomplete and imperfect. It grapples with many mysterious questions and can still not find satisfactory answers. For instance, how does the Standard Model explain gravity? Why do neutrinos have mass? What is dark matter and dark energy? The LHC is designed to collide protons at a maximum center-of-mass energy of 14 TeV, which is the energy region where the Standard Model is being explored [5]. We cannot predict at what energy order the Standard Model fails.

To give a better explanation, people are searching for new physics beyond the standard model in the LHC using different methods. The first one is to construct a new model that can fully explain everything and predict all the results that can be carried out. Some people are building new colliders to test new models or explore the energy range above 14 TeV. For example, the conceptual design report of the Circular Electron Positron Collider was submitted and adopted in 2018, and the conceptual design report of the Future Circular Collider (FCC) was submitted and accepted in 2020 [6][7]. Another commonly used method is to develop

Effective Field Theory (EFT) approaches to investigate the underlying new interactions between known particles. This paper focuses on the latter, exploring how EFT may be a powerful tool in exploring physics beyond the Standard Model and paying more attention to its application in the top quark part.

2 Standard Model Effective Field Theory

2.1 EFTs in a nutshell

Effective Field Theories (EFTs) are useful in physics, allowing for calculations without knowing the exact underlying theory [8]. The key part is to study physical phenomena at chosen lengths or energy scales without delving into the complexities of degrees of freedom at shorter distances or higher energy scales.

Effective Field Theory offers two different approaches: top-down and bottom-up. In the top-down approach, people start with a high-energy theory and then derive the theory at lower energy [9]. In contrast, the bottom-up approach is applied when a full theory is unknown or there's no applicable theory, and the Lagrangian density is constructed from scratch [9]. This process could respond to the experimental data and incorporate all possible interactions at the energy of interest. Hence, the bottom-up approaches allow for the development of a theory in response to the experimental results [9]. Wilson coefficients for bottom-up EFT are unspecified, allowing for flexibility in describing unknown physics. The Standard Model Effective Field Theory is a prime example of the theory constructed to capture the effects of high-energy physics beyond the Standard Model based on lower-energy experimental constraints [10].

The Wilson coefficient behaves as an effective coupling that quantifies the strength of high-order operators [11]. It can also show the effect of new physics beyond the energy scale in the experiment. The role of Wilson coefficients in SMEFT becomes important as it acts as the bridge between the unknown high-energy physics and the observable low-energy phenomena.

2.2 SMEFT

As discussed earlier, Standard Model Effective Field Theory (SMEFT) functions as a

'bottom-up' approach in EFTs. It operates under the specific assumption that the new physics occurs at some high energy scale beyond a certain threshold [12].

The SMEFT enables physicists to explore the potential impact of new physics by systematically incorporating high-energy effects into the SM description. It emphasizes observable effects while neglecting the substructure and degrees of freedom at shorter distances. This means that at energies below the scales at which new physics occurs, the details of the underlying high-energy structures become less relevant. Figure 1 illustrates this concept through the Feynman diagrams ranging from the SM to the SMEFT with decreasing energy. The diagram shows a hypothetical new particle Z' with a mass significantly larger than the Higgs mass $m_{Z'} \gg m_H$. At lower energies, the specific details of the intermediate particle become less relevant where the resolution is limited. By extending the SM, SMEFT allows the exploration of phenomena beyond the energy range the current experiment achieves. This involves the introduction of higher dimensional operators and new terms in the Lagrangian, which represent the potential interactions and effects that may arise at higher energy levels. These additional terms accommodate the possibility of new particles and interactions beyond those explained in the SM.

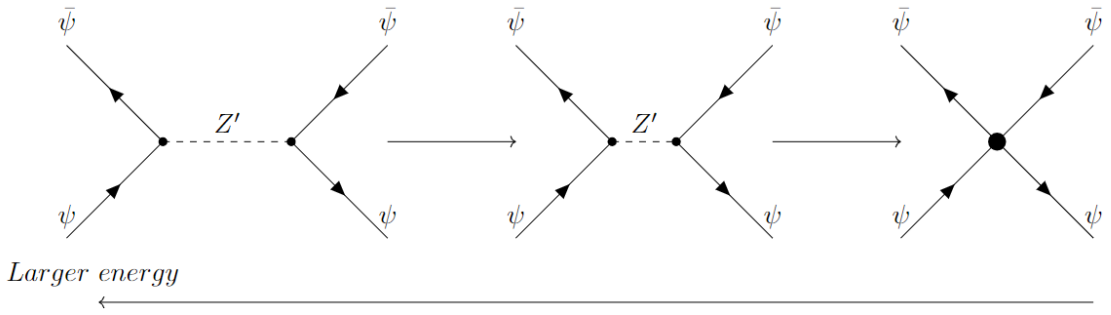

Figure 1. Feynman diagrams of a four-fermion process via an unknown heavy boson Z', showing the transition from higher to lower energy (left to right), and give the Feynman diagram in SMEFT. (Generated by Tikz-Feynman [13])

3 Constructing SMEFT

The Standard Model (SM) is the foundation for understanding fundamental particles. The mathematical formula to describe the SM is complex. However, it can be encapsulated in a concise way — Lagrangian. The Lagrangian of the SM $\mathcal{L}_{SM}$ is made up of four different parts,

each corresponding to different sectors of particle physics, which is usually expressed as

$$\mathcal{L}_{SM} = \mathcal{L}_f + \mathcal{L}_{gauge} + \mathcal{L}_{Yukawa} + \mathcal{L}_{\varphi}, \quad (1)$$

where the kinetic terms for fermions $\mathcal{L}_f$ and gauge bosons $\mathcal{L}_{gauge}$, the Yukawa coupling for fermion masses $\mathcal{L}_{Yukawa}$, and the Higgs potential $\mathcal{L}_{\varphi}$ [14]. It only contains dimension-two and dimension-four operators [15].

However, to cover potential effects beyond the SM range at a higher energy scale, the Standard Model Effective Field Theory (SMEFT) is introduced. It extends the SM Lagrangian by introducing higher dimensional operators ${O_i}^{(n)}$. The general form of an SMEFT Lagrangian can be expressed as

$$\mathcal{L}_{SMEFT} = \mathcal{L}_{SM} + \sum_{i,n\geq 5} \frac{c_i}{\Lambda^{n-4}} {O_i}^{(n)}, \quad (2)$$

where c_i represents the Wilson coefficients associated with each high-dimensional operator O_i, while Λ is the energy scale new physics is expected to appear, and n is the mass dimension of the operator [16]. The higher-dimensional operators included in the SMEFT framework can capture the effects of new physics beyond the SM. The SMEFT can be reduced to SM by decoupling heavy particles with masses of order Λ or larger [15]. The process of integrating these heavy fields from the experimental and theoretical prediction is involved in determining the coefficient c_i, once the underlying high-energy physics has been specified [15]. Hence, the gap between high-energy physics and low-energy observations is connected.

The first step to working out the SMEFT is to construct a complete Lagrangian with a basis of operators in each dimension. However, the formulation of the SMEFT Lagrangian contains an infinite number of interaction terms related to different dimensions, and it's impossible for us to calculate all the coefficients. In order to address this difficult task, power counting is introduced as an organizing tool that can establish the relative importance of various interaction terms [17]. The relevance of operators with greater mass diminishes as the energy scale decreases. Therefore, higher-dimensional operators contribute less significantly to observable phenomena. For a given scattering energy E, the contribution of different operators can be expressed as $c_i \left(\frac{E}{\Lambda}\right)^{n-4}$ [17].

For example, the effects of dimension-4 operators remain unsuppressed, while dimension-5 operators are suppressed by $\frac{E}{\Lambda}$, dimension-6 operators by $\left(\frac{E}{\Lambda}\right)^2$, and so on. Hence, lower-

dimensional operators have a more significant impact on experiment results when the energy scale is much smaller than the UV completion mass scale, that is, $E \ll \Lambda$ [17]. By applying this comprehension, it is possible to shorten the SMEFT Lagrangian to a specific dimension n and ignore the influence of higher-dimension terms. This simplifies the theoretical description while maintaining accuracy at lower energies.

Dimension-6 has received significant attention as it can contribute to a variety of physics areas, such as Higgs physics, electroweak precision observations, and so on. In contrast, although dimension-5 only contains a single operator, it can generate neutrino masses. However, neutrino mass poses significant experimental challenges to the current experiment that make the direct measurement more difficult [15]. Furthermore, the dimension-5 operator violates lepton numbers, leading to their exclusion for most of the experimental analysis [18].

In 2010, a set of independent dimension-6 operators known as 'Warsaw basis' was established in [15] following the work made in [19]. As indicated by Tables 1 and 2, this set contains a total of 59 independent dimension-6 operators, under the assumption of baryon and lepton conservation. These operators are divided into classes to describe different types of interactions that can occur within the SMEFT. These categories include 15 bosonic operators (X^3, $X^2\varphi^2$, φ^6, and $\varphi^4 D^2$), 19 two-fermion operators ($\psi^2\varphi^3$, $\psi^2 X\varphi$, $\psi^2\varphi^2 D$) and 25 four-fermion operators ($(\bar{L}L)\,(\bar{L}L)$, $(\bar{L}L)(\bar{R}R)$, $(\bar{R}R)(\bar{R}R)$, $(\bar{L}R)(\bar{L}R)$, $(\bar{L}R)(\bar{R}L)$), each of these operator indicates a specific interaction.

X^3		φ^6 and $\varphi^4 D^2$		$\psi^2\varphi^3$	
Q_G	$f^{ABC}G_\mu^{A\nu}G_\nu^{B\rho}G_\rho^{C\mu}$	Q_φ	$(\varphi^\dagger\varphi)^3$	$Q_{e\varphi}$	$(\varphi^\dagger\varphi)(\bar{l}_p e_r\varphi)$
$Q_{\widetilde{G}}$	$f^{ABC}\widetilde{G}_\mu^{A\nu}G_\nu^{B\rho}G_\rho^{C\mu}$	$Q_{\varphi\Box}$	$(\varphi^\dagger\varphi)\Box(\varphi^\dagger\varphi)$	$Q_{u\varphi}$	$(\varphi^\dagger\varphi)(\bar{q}_p u_r\widetilde{\varphi})$
Q_W	$\varepsilon^{IJK}W_\mu^{I\nu}W_\nu^{J\rho}W_\rho^{K\mu}$	$Q_{\varphi D}$	$\left(\varphi^\dagger D^\mu\varphi\right)^\star\left(\varphi^\dagger D_\mu\varphi\right)$	$Q_{d\varphi}$	$(\varphi^\dagger\varphi)(\bar{q}_p d_r\varphi)$
$Q_{\widetilde{W}}$	$\varepsilon^{IJK}\widetilde{W}_\mu^{I\nu}W_\nu^{J\rho}W_\rho^{K\mu}$				
$X^2\varphi^2$		$\psi^2 X\varphi$		$\psi^2\varphi^2 D$	
$Q_{\varphi G}$	$\varphi^\dagger\varphi G_{\mu\nu}^A G^{A\mu\nu}$	Q_{eW}	$(\bar{l}_p\sigma^{\mu\nu}e_r)\tau^I\varphi W_{\mu\nu}^I$	$Q_{\varphi l}^{(1)}$	$(\varphi^\dagger i\overleftrightarrow{D}_\mu\varphi)(\bar{l}_p\gamma^\mu l_r)$
$Q_{\varphi\widetilde{G}}$	$\varphi^\dagger\varphi\widetilde{G}_{\mu\nu}^A G^{A\mu\nu}$	Q_{eB}	$(\bar{l}_p\sigma^{\mu\nu}e_r)\varphi B_{\mu\nu}$	$Q_{\varphi l}^{(3)}$	$(\varphi^\dagger i\overleftrightarrow{D}_\mu^I\varphi)(\bar{l}_p\tau^I\gamma^\mu l_r)$
$Q_{\varphi W}$	$\varphi^\dagger\varphi W_{\mu\nu}^I W^{I\mu\nu}$	Q_{uG}	$(\bar{q}_p\sigma^{\mu\nu}T^A u_r)\widetilde{\varphi}G_{\mu\nu}^A$	$Q_{\varphi e}$	$(\varphi^\dagger i\overleftrightarrow{D}_\mu\varphi)(\bar{e}_p\gamma^\mu e_r)$
$Q_{\varphi\widetilde{W}}$	$\varphi^\dagger\varphi\widetilde{W}_{\mu\nu}^I W^{I\mu\nu}$	Q_{uW}	$(\bar{q}_p\sigma^{\mu\nu}u_r)\tau^I\widetilde{\varphi}W_{\mu\nu}^I$	$Q_{\varphi q}^{(1)}$	$(\varphi^\dagger i\overleftrightarrow{D}_\mu\varphi)(\bar{q}_p\gamma^\mu q_r)$
$Q_{\varphi B}$	$\varphi^\dagger\varphi B_{\mu\nu}B^{\mu\nu}$	Q_{uB}	$(\bar{q}_p\sigma^{\mu\nu}u_r)\widetilde{\varphi}B_{\mu\nu}$	$Q_{\varphi q}^{(3)}$	$(\varphi^\dagger i\overleftrightarrow{D}_\mu^I\varphi)(\bar{q}_p\tau^I\gamma^\mu q_r)$
$Q_{\varphi\widetilde{B}}$	$\varphi^\dagger\varphi\widetilde{B}_{\mu\nu}B^{\mu\nu}$	Q_{dG}	$(\bar{q}_p\sigma^{\mu\nu}T^A d_r)\varphi G_{\mu\nu}^A$	$Q_{\varphi u}$	$(\varphi^\dagger i\overleftrightarrow{D}_\mu\varphi)(\bar{u}_p\gamma^\mu u_r)$
$Q_{\varphi WB}$	$\varphi^\dagger\tau^I\varphi W_{\mu\nu}^I B^{\mu\nu}$	Q_{dW}	$(\bar{q}_p\sigma^{\mu\nu}d_r)\tau^I\varphi W_{\mu\nu}^I$	$Q_{\varphi d}$	$(\varphi^\dagger i\overleftrightarrow{D}_\mu\varphi)(\bar{d}_p\gamma^\mu d_r)$
$Q_{\varphi\widetilde{W}B}$	$\varphi^\dagger\tau^I\varphi\widetilde{W}_{\mu\nu}^I B^{\mu\nu}$	Q_{dB}	$(\bar{q}_p\sigma^{\mu\nu}d_r)\varphi B_{\mu\nu}$	$Q_{\varphi ud}$	$i(\widetilde{\varphi}^\dagger D_\mu\varphi)(\bar{u}_p\gamma^\mu d_r)$

Table 1. Dimension-six operators in the SMEFT without the four-fermion operators [15].

$(\bar{L}L)(\bar{L}L)$		$(\bar{R}R)(\bar{R}R)$		$(\bar{L}L)(\bar{R}R)$	
Q_{ll}	$(\bar{l}_p\gamma_\mu l_r)(\bar{l}_s\gamma^\mu l_t)$	Q_{ee}	$(\bar{e}_p\gamma_\mu e_r)(\bar{e}_s\gamma^\mu e_t)$	Q_{le}	$(\bar{l}_p\gamma_\mu l_r)(\bar{e}_s\gamma^\mu e_t)$
$Q_{qq}^{(1)}$	$(\bar{q}_p\gamma_\mu q_r)(\bar{q}_s\gamma^\mu q_t)$	Q_{uu}	$(\bar{u}_p\gamma_\mu u_r)(\bar{u}_s\gamma^\mu u_t)$	Q_{lu}	$(\bar{l}_p\gamma_\mu l_r)(\bar{u}_s\gamma^\mu u_t)$
$Q_{qq}^{(3)}$	$(\bar{q}_p\gamma_\mu\tau^I q_r)(\bar{q}_s\gamma^\mu\tau^I q_t)$	Q_{dd}	$(\bar{d}_p\gamma_\mu d_r)(\bar{d}_s\gamma^\mu d_t)$	Q_{ld}	$(\bar{l}_p\gamma_\mu l_r)(\bar{d}_s\gamma^\mu d_t)$
$Q_{lq}^{(1)}$	$(\bar{l}_p\gamma_\mu l_r)(\bar{q}_s\gamma^\mu q_t)$	Q_{eu}	$(\bar{e}_p\gamma_\mu e_r)(\bar{u}_s\gamma^\mu u_t)$	Q_{qe}	$(\bar{q}_p\gamma_\mu q_r)(\bar{e}_s\gamma^\mu e_t)$
$Q_{lq}^{(3)}$	$(\bar{l}_p\gamma_\mu\tau^I l_r)(\bar{q}_s\gamma^\mu\tau^I q_t)$	Q_{ed}	$(\bar{e}_p\gamma_\mu e_r)(\bar{d}_s\gamma^\mu d_t)$	$Q_{qu}^{(1)}$	$(\bar{q}_p\gamma_\mu q_r)(\bar{u}_s\gamma^\mu u_t)$
		$Q_{ud}^{(1)}$	$(\bar{u}_p\gamma_\mu u_r)(\bar{d}_s\gamma^\mu d_t)$	$Q_{qu}^{(8)}$	$(\bar{q}_p\gamma_\mu T^A q_r)(\bar{u}_s\gamma^\mu T^A u_t)$
		$Q_{ud}^{(8)}$	$(\bar{u}_p\gamma_\mu T^A u_r)(\bar{d}_s\gamma^\mu T^A d_t)$	$Q_{qd}^{(1)}$	$(\bar{q}_p\gamma_\mu q_r)(\bar{d}_s\gamma^\mu d_t)$
				$Q_{qd}^{(8)}$	$(\bar{q}_p\gamma_\mu T^A q_r)(\bar{d}_s\gamma^\mu T^A d_t)$
$(\bar{L}R)(\bar{R}L)$ and $(\bar{L}R)(\bar{L}R)$		B-violating			
Q_{ledq}	$(\bar{l}_p^j e_r)(\bar{d}_s q_t^j)$	Q_{duq}	$\varepsilon^{\alpha\beta\gamma}\varepsilon_{jk}\left[(d_p^\alpha)^T C u_r^\beta\right]\left[(q_s^{\gamma j})^T C l_t^k\right]$		
$Q_{quqd}^{(1)}$	$(\bar{q}_p^j u_r)\varepsilon_{jk}(\bar{q}_s^k d_t)$	Q_{qqu}	$\varepsilon^{\alpha\beta\gamma}\varepsilon_{jk}\left[(q_p^{\alpha j})^T C q_r^{\beta k}\right]\left[(u_s^\gamma)^T C e_t\right]$		
$Q_{quqd}^{(8)}$	$(\bar{q}_p^j T^A u_r)\varepsilon_{jk}(\bar{q}_s^k T^A d_t)$	$Q_{qqq}^{(1)}$	$\varepsilon^{\alpha\beta\gamma}\varepsilon_{jk}\varepsilon_{mn}\left[(q_p^{\alpha j})^T C q_r^{\beta k}\right]\left[(q_s^{\gamma m})^T C l_t^n\right]$		
$Q_{lequ}^{(1)}$	$(\bar{l}_p^j e_r)\varepsilon_{jk}(\bar{q}_s^k u_t)$	$Q_{qqq}^{(3)}$	$\varepsilon^{\alpha\beta\gamma}(\tau^I\varepsilon)_{jk}(\tau^I\varepsilon)_{mn}\left[(q_p^{\alpha j})^T C q_r^{\beta k}\right]\left[(q_s^{\gamma m})^T C l_t^n\right]$		
$Q_{lequ}^{(3)}$	$(\bar{l}_p^j\sigma_{\mu\nu}e_r)\varepsilon_{jk}(\bar{q}_s^k\sigma^{\mu\nu}u_t)$	Q_{duu}	$\varepsilon^{\alpha\beta\gamma}\left[(d_p^\alpha)^T C u_r^\beta\right]\left[(u_s^\gamma)^T C e_t\right]$		

Table 2. Dimension-6 Four-fermion operators [15].

For example, the bosonic operator $Q_{\varphi G}$ may represent the interactions between the Higgs field and the gluon, two possible interactions can be depicted as in Figure 2. Similarly, the operator

$Q_{\varphi e}$ represents the interaction between the Higgs field and the electrons e. The presentation of this interaction through the Feynman diagram could be visualized in Figure 3. An example of a four-fermion operator Q_{uu} is shown in Figure 4, indicating the interaction between up-quarks. Once the Lagrangian is constructed, the Wilson coefficient for each operator can be found by experimental and theoretical prediction. In this process, it required different experimental information to constrain all Wilson coefficients c_i. However, excluding baryon and lepton conservation, there are a total of 2499 dimension-6 operators. Therefore, it is impossible to determine all relevant coefficients. This situation requires the prioritization of specific interactions to constrain, rather than attempting to fit all coefficients simultaneously.

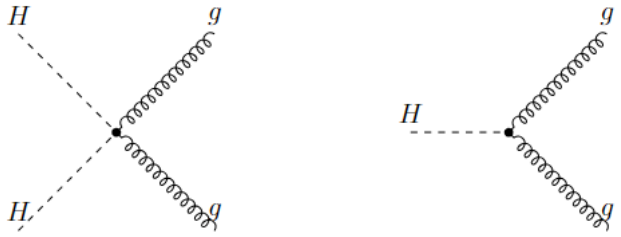

Figure 2: Two Feynman diagrams given by the $Q_{\varphi G}$ operator, generated by Tikz-Feynman [13].

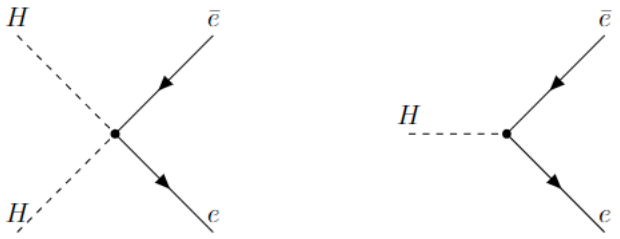

Figure 3: The Feynman diagrams depict the interaction between two electrons and the Higgs field, indicating the $Q_{\varphi e}$ operator, generated by Tikz-Feynman [13].

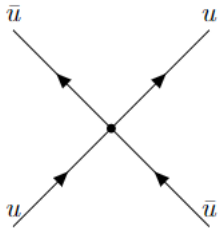

Figure 4: The Feynman diagram depicts the interaction between two up-quarks, indicating the Q_{uu} operator, generated by Tikz-Feynman [13].

4 SMEFT in top sector

In the Standard Model Effective Field Theory (SMEFT), the top quark sector is especially interesting because the top quark is a key part in the dynamics of the SM and might be able to sense new physics beyond the SM.

The top quarks, being the heaviest known fermion particle, have a significant impact on a variety of high-energy processes and are highly susceptible to the effects of new physics. Higher-dimensional operators in the SMEFT introduce modifications that affect processes involving top-quarks, such as top quark production and decay. By incorporating these operators into the analysis, physicists are able to investigate deviations from the SM predictions, which creates an opportunity to potentially uncover signs of new physics. The top quark's large mass makes it especially sensitive to effects from physics beyond the energy scales probed by current experiments.

There are multiple processes related to the production of top quarks, the main two mechanisms are top quark pair production and single top quark production.

The primary production mechanisms for the top quark pairs ($\bar{t}t$) in the Large Hadron Collider (LHC), which account for more than 90% of the cross section, are through strong interactions. Highly energetic gluons decay to generate $\bar{t}t$ pairs as shown in Figure 5 [20]. Top quark was first discovered by this process in 1995 [21]. Another main process that would produce top quark pairs is quark- antiquark annihilation, as shown in Figure 5. In addition, top-quark pairs can also be produced by the mechanism of decay of an intermediate photon or Z-boson with less frequency.

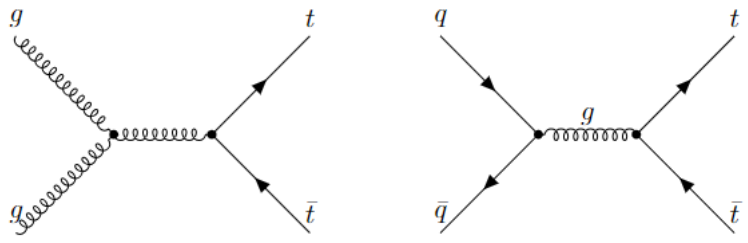

Figure 5: Feynman diagrams show the production of top quark pairs by gluon-fusion (left) and quark-antiquark annihilation (right), which was generated by Tikz-Feynman [13].

Single top quark can also be generated via electroweak interaction. [22] This can happen through many different channels. An illustration of this can be seen in Figure 6, where the

term ‘s-channel’ indicates an intermediate W-boson decays into a top quark and a bottom antiquark. The ‘t-channel’ means a bottom quark (or antiquark) interacts with an up- or down-type quark and transforms into a top quark (or antiquark) via the exchange of a W-boson.

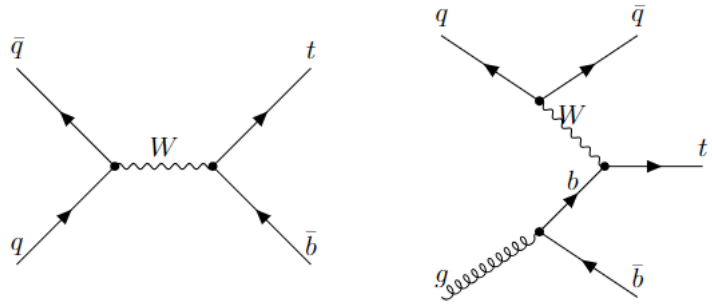

Figure 6: Feynman diagrams show the s-channel (left) and the t-channel (right), which were generated by Tikz-Feynman [13].

Due to the huge mass of the top quark, it has an extremely short lifetime, only $5 \times 10^{-25} s$ [23]. The massive nature of the top quark results in a rapid decay process before it can form other hadrons. The primary decay mode of the top quark is through weak interaction, which leads to the production of a W boson and a bottom quark. The charged W-boson then decays further to produce various possible channels, including lepton pairs or quark pairs, an example is given in Figure 7 [23].

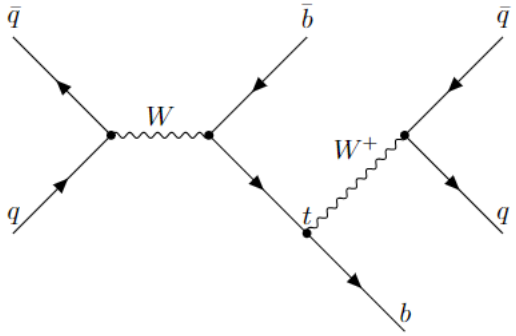

Figure 7: The Feynman diagrams illustrate the top quark decay process to a W boson (W^+) and a bottom quark. The W bosons subsequently decay to quark-antiquark pairs. (Generated by Tikz-Feynman [13])

5 Examples of Top Quark SMEFT Studies

Experiments at the Large Hadron Collider (LHC), such as ATLAS and CMS, have extensively studied top quark properties at higher collision energies. They have explored rare top quark

processes, top quark couplings to other particles, and searched for new physics phenomena related to top quark interactions. Two experimental analyses were introduced as new physics explored examples using SMEFT in this section.

5.1 Single Top Quark Production and EFT interpretation

An analysis conducted in 2022 studied the production of a single top quark generated through the t-channel within the framework of the SMEFT [24]. The analysis is based on the proton-proton collision data collected at the ATLAS with a center-of-mass energy of 13 TeV.

In the t-channel production of single top quarks or antiquarks at $\sqrt{s} = 13TeV$, two primary subprocesses contribute at Leading Order (LO), as illustrated in Figure 8. These involve the exchange of a virtual W boson by the incoming light-flavor quark, resulting in the production of a top quark (t) or a top antiquark ($\bar{t}$), along with a recoiled light-flavor quark q, termed the spectator quark. The dominant subprocesses involve the production of a down (up) quark and a top quark (antiquark) from a down (up) quark, while the subdominant subprocesses involve the scattering of a down (up) antiquark from a bottom quark (antiquark) to produce a down (up) antiquark and a top quark (antiquark).

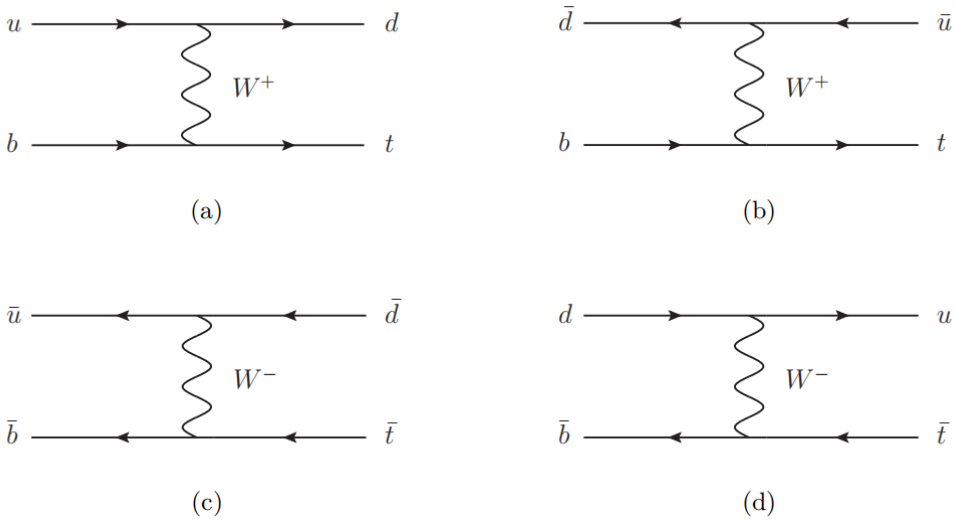

Figure 8: Feynman diagrams show the single top quark production by t-channel. (a)(d) are responsible for the dominant subprocesses while (c)(d) are responsible for the subdominant subprocess (generated by Tikz-Feynman [13]).

In these processes, the spin of the top quark (antiquark) aligns with the down quark (antiquark)

along the direction of the incoming quark or the spectator quark. The analysis utilized the decay mode of the top quark $t \to Wb \to b\ell^+\nu$ and the charge-conjugate decay mode of the top antiquark. The spin information of the top quark could be transferred to the decay products, allowing for extraction through their angular distributions. Hence, a direct measurement of top quark and top antiquark polarization vectors was presented by fitting a joint distribution of charged-lepton momentum direction cosines in the top quark frame.

Additionally, the normalized angular differential cross sections of top quark and antiquark production were expressed in terms of the angles of charged lepton in the top-quark and top antiquark events separately and combined. These measurements were used in the framework of Effective Field Theory (EFT) to constrain the complex Wilson coefficients. Particularly, the inclusive measurements were applied to determine bounds on the complex Wilson coefficient of the O_{tW} operator. The O operator mentioned here actually corresponds to the previous Q operator mentioned in Tables 1 and 2, although using a different notation in this analysis.

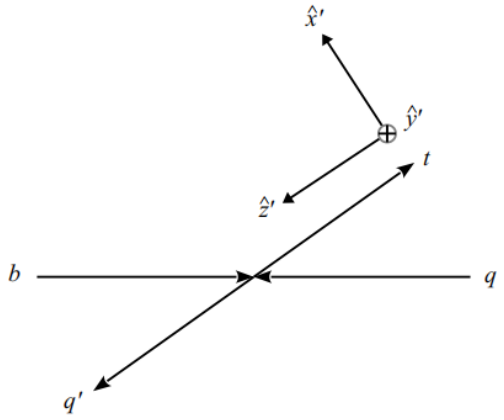

Figure 9: The diagram illustrates the orthogonal direction $\hat{x}'$, $\hat{y}'$ and $\hat{z}'$ used in this analysis [24].

It is necessary to develop a Lagrangian within the SMEFT framework. Given that dimension-5 operators don't contribute to the production or decay of the top quark [25], this analysis mainly focused on the dimension-6 operators and their associated Wilson coefficient. The operator O_{tW} was the only one that influences the polarization of top quarks in this analysis. The polarization is significantly affected by the O_{tW} operator and its complex coefficients C_{tW} and C_{itW}. The real part of the Wilson coefficient C_{tW} mostly affect $P_{x'}$ and the imaginary part C_{itW} affect $P_{y'}$, where the $\hat{x}'$, $\hat{y}'$ and $\hat{z}'$ direction are defined in the Figure 9. A non-zero

C_{itW} value may indicate a non-SM CP violation in the tWb vertex.

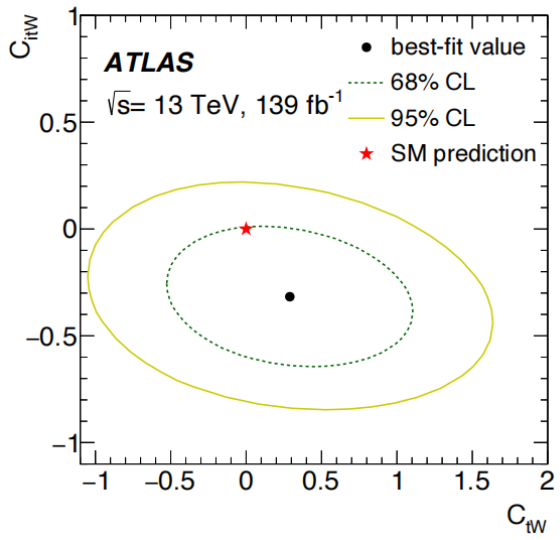

Figure 10: The observed best-fit value (represented by a dot) for the Wilson coefficient C_{tW} and C_{itW}. Uncertainty contour at 68% confidence level is shown by the green dashed lines, while the uncertainty contour at 95% confidence level is represented by the yellow solid lines. The red star donated the SM prediction [24].

The obtained results for fitting the coefficients simultaneously were $C_{tW} = 0.3 \pm 0.6\ (1.1)$ and $C_{itW} = -0.3 \pm 0.2\ (0.5)$ to the 68% (95%) level of confidence, which are presented in Figure 10. The red star representing the SM prediction lies within the 95% level of confidence contour, so the values are consistent with the SM prediction. The EFT model was fitted with the best fit values using the Madgraph5-aMC@NLO+PYTHIA8 generator, and the resulting values with a confidence level of 95% were determined to be $C_{tW} \in [-0.9, 1.4]$ and $C_{itW} \in [-0.8, 0.2]$. For each coefficient, the result is also obtained by setting the other coefficient to zero. The bounds on C_{itW} in this paper improved the previous ATLAS result [26][27].

5.2 $t\bar{t}Z$ Production and EFT interpretation

Another analysis example that was conducted in September 2023 presents a study of the joint production of top quark-antiquark pairs and Z bosons ($t\bar{t}Z$) using 170 fb^{-1} data collected by the ATLAS experiment between 2015 and 2018 [28]. The research did not restrict itself to the decay of top quark channels, it focused on the decay of Z bosons into electrons and muons. It imposed constraints on dimension-6 Effective Field Theory (EFT) operators that are related to

the top quark and the Z boson within the limitation of SMEFT by measuring the $t\bar{t}Z$ inclusive and differential cross-sections.

The production of the top quark-antiquark pair with the Z boson at the LHC is considered a rare process within the framework of the SM. This process is particularly noteworthy as it produces a variety of multilepton final states and makes a significant contribution as a background for the measurements of other key SM processes at the LHC. For example, the analysis must consider the influence of $t\bar{t}Z$ processes when studying the generation of $t\bar{t}$ pairs associated with the Higgs boson and $t\bar{t}$ production [29].

This analysis focused on three multilepton final states with two (2ℓ), three (3ℓ), and four (4ℓ) leptons, respectively, while the differential measurement is only performed in the 3ℓ and 4ℓ channels. The dilepton channel is ignored here due to its high background contamination. Once the differential distributions, such as the transverse momentum of top quark, were obtained, they were parameterized and used as input for the EFT interpretation.

Based on the EFT interpretations, the dependance of an observable, such as an inclusive or differential cross-section, denoted as O, on a specific Wilson coefficient represented as C, can be expressed or parameterized as follows:

$$O = O_{SM} + \sum_i C_i A_i + \sum_{i,j} C_i C_j B_{ij}, \quad (3)$$

where O_{SM} stands for the expected value of the observable in the SM in the absence of new physics effects. A_i are the linear terms representing the interference between the SM and the SMEFT. B_{ij} are the quadratic terms that represent the pure SMEFT contribution, if $i = j$, it indicates a pure quadratic term, while if not, it donates a cross-term.

In the same way, the dimension-5 operator was not used in this analysis to build the SMEFT Lagrangian because it goes against the conservation of lepton numbers. In this analysis, 20 top-quark related operators are considered, they can be divided into top-boson operators and four-quark operators. By fitting in the 3ℓ and 4ℓ signal channels, the coefficients of these two types of operators were fitted independently.

The Feynman diagrams showing the specific examples of interactions associated with their operators are given in Figure 11. The operator Q_{tG} represents the interaction where a top quark pair generates a Higgs boson and a gluon. The Q_{tB} operator represents the interaction where a top quark pair produces either a photon or a Z boson. Notably, three of the Wilson

coefficients corresponding to their operators Q_{tW}, Q_{tB}, Q_{tG} have distinct imaginary part, therefore, they are shown separately shown in Figure 12.

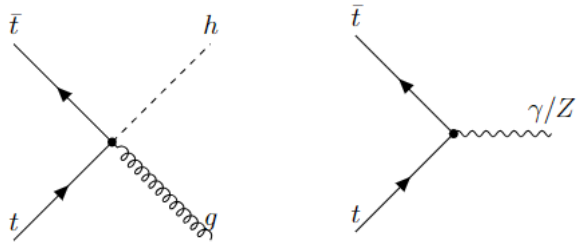

Figure 11: Feynman diagrams illustrating the interactions given by the Q_{tG} operator (left) and Q_{tB} operator (right), which were generated by Tikz-Feynman [13].

Two fitting approaches were employed. The first one involved the normal fit using full quadratic parametrization in equation (3), where all linear, quadratic, and cross-terms were used simultaneously across all operators. The second fitting only considered linear terms to reflect the importance of interference terms. In addition, independent full quadratic fits were performed for each operator, which held all other coefficients constant at zero in order to compare with other analyses.

However, the linear fitting results for some certain operators were not reported, such as the imaginary parts of the Wilson coefficients of C_{tG} and C_{tW}, and some color-singlet four-quark operators. This situation occurred because these operators did not interfere with the SM. Therefore, these specific interference terms were considered negligible at the LO level, and the linear fitting results of these operators could not be represented.

The results for all Wilson coefficients are shown in Figure 12. The observation is that all coefficients with a 95% level of confidence include the value of zero, indicating no clear deviation from the prediction of the SM. In other words, the uncertainty interval or level of confidence interval includes a value of zero, indicating that there is no significant evidence for new physics beyond the SM.

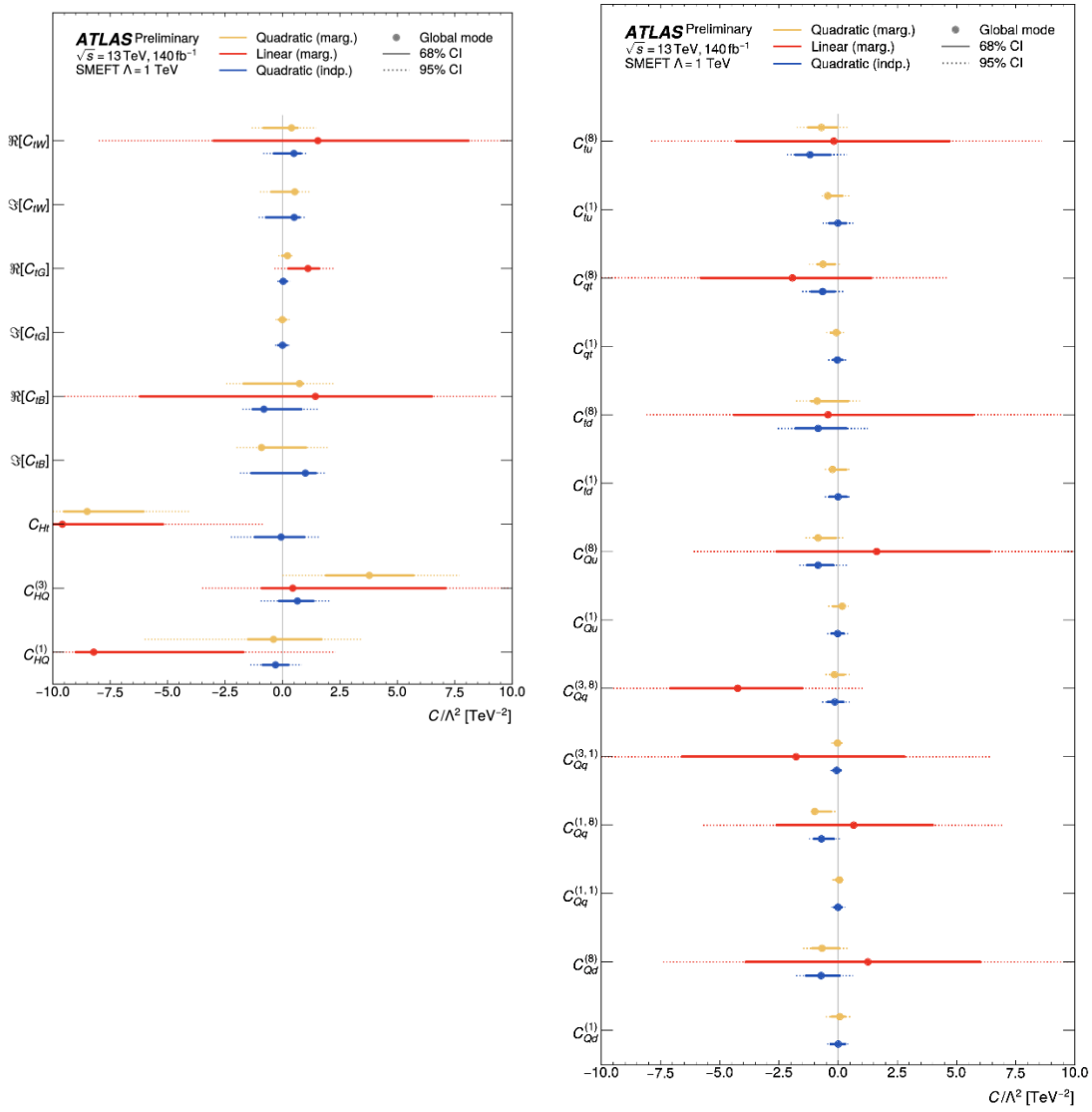

Figure 12: The result of the Wilson coefficients with their 68% and 95% level of confidence obtained in the top-boson scenario (left) and the four-quark scenario (right) for the marginalized quadratic and linear fits and independent quadratic fits [28].

6 Conclusion

While the Standard Model has emerged as an exceptional framework for understanding particle physics phenomena, it is widely recognized that the SM may not be the complete picture, especially at higher energy scales where new physics may appear. In order to find out the potential deviation beyond the SM, the Standard Model Effective Field Theory (SMEFT) works as a general approach. SMEFTs extend the SM by incorporating high dimensional operators, which allow us to explore new physics phenomena at energy scales beyond the

experiments.

In the field of SMEFT, the top quark sector has great significance because top quarks are sensitive to new physics due to their huge mass. The study of high-dimensional operators related to top quarks in SMEFT provides a way to identify deviations from SM predictions and reveal signs of new physics. Two examples of analysis based on the data collected by ATLAS demonstrate the application of SMEFT to the top quark sector. Two analyses constrain the Wilson coefficient in different ways. The first one focused on the production of a single top quark in the t-channel, and obtained the polarization of the top quark (antiquark) through the angle of the lepton produced by the decay of the top quark (antiquark), which is then used to constrain Wilson coefficients. The second constrained different top-quark-related processes by different fitting methods at various scenarios. Thus far, all results to date have been consistent with SM, indicating that SMEFT is a highly effective method as it can be implemented in a variety of ways. Although both experimental analyses do not shown deviations from the SM, the application of SMEFT gives an opportunity to explore beyond the SM. The SMEFT not only refines our understanding of particle interactions but also exploits potential breakthroughs in fundamental physics.

Reference

[1] Gino Isidori, Felix Wilsch, Daniel Wyler (2023), 'The Standard Model effective field theory at work', *arXiv:2303.16922v2 [Hep-Ph]*.

[2] Arnison, Geoffrey, Astbury, Alan, *et al.* (1983), 'Experimental observation of isolated large transverse energy electrons with associated missing energy at $\sqrt{s} = 540GeV$', *Physics Letters B*, 122 (1), pp. 103-116.

[3] Arnison, G. *et al.* (1983), 'Experimental observation of lepton pairs of invariant mass around 95 $\mathrm{Gev/c^2}$ at the CERN SPS collider', *Physics Letters B*, 126(5), pp. 398–410.

[4] Aaltonen, T. *et al.* (2012), 'Evidence for a particle produced in association with weak bosons and decaying to a bottom-antibottom quark pair in Higgs boson searches at the Tevatron', *Physical Review Letters*, 109(7).

[5] CERN, "*Restarting the LHC: Why 13 TeV?*" Available at: https://home.cern/science/engineering/restarting-lhc-why-13-tev, accessed date (10/11/2023).

[6] Circular Electron Positron Collider, "*The CEPC project*", Available at: http://cepc.ihep.ac.cn/intro.html, accessed date (19/11/2023).

[7] CERN, "*Future Circular Collider*" Available at: https://home.cern/science/accelerators/future-circular-collider, accessed date (11/11/2023).

[8] Davidson S. *et al.* (2017), *Effective Field Theory in Particle Physics and Cosmology: Lecture Notes of the Les Houches Summer School: Volume 108, session CVIII*, Oxford University Press.

[9] Crowther, K. (2013), 'Emergent spacetime according to effective field theory: From top-down and bottom-up', *Studies in History and Philosophy of Modern Physics*, 44(3), pp. 321–328.

[10] Massimiliano G. *et al*. (2017), 'Effective Field Theory for Higgs properties parametrisation: the transverse momentum spectrum case', *arXiv:1705.05143v1 [hep-ph]*.

[11] Tarek Abouelfadl Mohamed, A. (2020). *Beyond the Standard Model: The Effective Field Theory Approach. In: Measurement of Higgs Boson Production Cross Sections in the Diphoton Channel*. Springer Theses. Springer, Cham.

[12] Passarino, G. (2017) 'SMEFT, a theory for SM Deviations', *Proceedings of 38th*

International Conference on High Energy Physics — PoS(ICHEP2016).

[13] Ellis, J. (2016) 'TikZ-Feynman: Feynman diagrams with TikZ', *arXiv:1601.05437v1 [hep-ph]*.

[14] Langacker, P. (2021), *The standard model and beyond*, 2nd Edition, CRC Press, Taylor & Francis Group.

[15] Grzadkowski, B. *et al.* (2010) 'Dimension-six terms in the Standard Model Lagrangian', *Journal of High Energy Physics*, 85(2010).

[16] Brian, H. *et al.* (2014) 'How to use the Standard Model effective field theory', *arXiv:1412.1837v2 [hep-ph]*.

[17] Falkowski, A. (2023) 'Lectures on SMEFT', *The European Physical Journal C*, 83(7).

[18] Andreas Helset, Andrew Kobach (2019) 'Baryon Number, Lepton Number, and Operator Dimension in the SMEFT with Flavor Symmetries', *arXiv:1909.05853v1 [hep-ph]*.

[19] Buchmüller, W. and Wyler, D. (1986) 'Effective lagrangian analysis of new interactions and flavour conservation', *Nuclear Physics B*, 268(3–4), pp. 621–653.

[20] Moore, Liam Ronald (2016) 'Top quark physics in the Standard Model Effective Field Theory'. *PhD thesis, University of Glasgow*.

[21] F. Abe et al. (CDF Collaboration), 'Observation of Top Quark Production in $p\,p$ Collisions with the Collider Detector at Fermilab', *Phys. Rev. Lett*. 74, 2626.

[22] D0 Collaboration: V.M. Abazov, *et al.* (2009) 'Observation of Single Top-Quark Production', *arXiv:0903.0850v2 [hep-ex]*.

[23] Frederic Deliot (2011), 'Top Quark Physics At Hadron Colliders', *arXiv:1111.6274v1 [hep-ex]*.

[24] ATLAS Collaboration (2022), 'Measurement of the polarisation of single top quarks and antiquarks produced in the t-channel at $\sqrt{s} = 13TeV$ TeV and bounds on the tWb dipole operator from the ATLAS experiment', *arXiv:2202.11382v2 [hep-ex]*.

[25] Zhang, C. and Willenbrock, S. (2011) 'Effective-field-theory approach to top-quark production and decay', *Physical Review D*, 83(3).

[26] ATLAS collaboration (2017), 'Analysis of the Wtb vertex from the measurement of triple-differential angular decay rates of single top quarks produced in the t-channel at $\sqrt{s} = 8TeV$, with the ATLAS detector', *arXiv:1707.05393v2 [hep-ex]*.

[27] Déliot, F. *et al.* (2018), 'Global constraints on top quark anomalous couplings', *Physical Review D*, 97(1).

[28] ATLAS collaboration (2023), 'Inclusive and differential cross section measurements of $t\bar{t}Z$ production in $p\,p$ collisions at $\sqrt{s} = 13TeV$ with the ATLAS detector, including EFT and spin correlations interpretations', https://cds.cern.ch/record/2873519, assessed date (14/11/2023).

[29] CMS Collaboration (2020), 'Measurement of top quark pair production in association with a Z boson in proton-proton collisions at $\sqrt{s} = 13TeV$', *arXiv:1907.11270v2 [hep-ex]*.